processes

MDPI

Article

Evaluation of Tight Gas Reservoirs and Characteristics of Fracture Development: A Case Study of the He 8 Member in the Western Sulige Area, Ordos Basin

Zhaoyu Zhang [1], Jingong Zhang [2,*], Zhiqiang Chen [1] and Wanting Wang [3]

[1] Department of Geology, Northwest University, Xi'an 710069, China; 18463537895@163.com (Z.Z.)
[2] State Key Laboratory of Continental Evolution and Early Life, Xi'an 710069, China
[3] Shaanxi Coalfield Geophysical Surveying and Mapping Co., Ltd., Xi'an 710005, China
* Correspondence: zhangjgong@126.com

Abstract

This study focuses on the tight sandstone reservoirs of the He 8 Member (Lower Permian Shihezi Formation) in the western Sulige area, Ordos Basin. Multiple analytical methods were integrated, including core observation, thin-section analysis, X-ray diffraction (XRD), and rock mechanics experiments, to systematically evaluate the reservoir's petrology, pore microstructure, physical properties, and fracture formation mechanisms. Results indicate that the reservoir is primarily composed of quartz arenite (78%), characterized by low porosity (avg. 5.5%) and permeability (avg. 0.15 mD). The pore system comprises dissolution pores, lithic dissolution pores, intergranular pores, and intercrystalline pores. Depositional microfacies significantly influence reservoir quality. Subaqueous distributary channel sands exhibit the best properties (porosity > 5%), followed by mouth bar deposits. The reservoir experienced intense compaction and siliceous cementation, which considerably reduced primary porosity. In contrast, dissolution and tectonic fracturing processes significantly enhanced reservoir quality. Rock mechanics tests reveal that highly heterogeneous rocks are more prone to fracturing under differential stress (σ_1–σ_3). These fractures considerably improve the flow capacity of tight reservoirs.

Keywords: tight sandstone gas; Ordos Basin; Sulige gas field; fracture development characteristics; reservoir evaluation

check for updates

Academic Editors: Adebayo Abdulrauf, Liwu Jiang and Ahmed Al-Yaseri

Received: 6 August 2025
Revised: 25 August 2025
Accepted: 2 September 2025
Published: 4 September 2025

Citation: Zhang, Z.; Zhang, J.; Chen, Z.; Wang, W. Evaluation of Tight Gas Reservoirs and Characteristics of Fracture Development: A Case Study of the He 8 Member in the Western Sulige Area, Ordos Basin. *Processes* **2025**, *13*, 2838. https://doi.org/10.3390/pr13092838

Copyright: © 2025 by the authors. Licensee MDPI, Basel, Switzerland. This article is an open access article distributed under the terms and conditions of the Creative Commons Attribution (CC BY) license (https://creativecommons.org/licenses/by/4.0/).

1. Introduction

Unconventional oil and gas refer to continuously distributed hydrocarbon resources that cannot produce at commercial flow rates using conventional techniques without enhanced recovery methods to improve reservoir permeability or fluid mobility [1,2]. Major types include shale oil and gas, tight oil and gas, coalbed methane, gas hydrates, and oil shale. Although characterized by source-reservoir integration, complex accumulation mechanisms, high drilling costs, and technically challenging development, unconventional resources demonstrate extensive distribution, substantial resource potential, and promising exploration prospects [3–6]. Tight sandstone gas constitutes a vital component of unconventional natural gas systems, characterized by abundant reserves and widespread distribution [7]. Globally, over 70 tight gas basins have been identified or inferred, with total resources exceeding 210×10^{12} m^3. More than 60% of these resources are concentrated in Asia-Pacific, North America, and Latin America [8,9]. While tight hydrocarbon R&D

originated in North America, China has rapidly emerged as the world's third-largest tight gas producer despite its late industrial start [10].

With escalating energy demands outpacing conventional production, the petroleum industry urgently requires expanded unconventional resource exploration. Current research on tight gas reservoirs primarily focuses on static parameters, provenance analysis, and accumulation characteristics, while comprehensive reservoir evaluations have received comparatively less attention [11]. Furthermore, studies of fractures in tight reservoirs frequently emphasize geometric morphology, size classification, and occurrence types, but often neglect their formation mechanisms [12]. This study investigates the tight sandstone reservoirs of the Permian He 8 Member in the western Sulige area of the Ordos Basin. An integrated analysis of reservoir characteristics, controlling factors, and fracture formation mechanisms is presented.

2. Geological Overview of the Study Area

The Ordos Basin, ranking as China's second-largest sedimentary basin with an area of 25×10^4 km^2, spans the provinces of Gansu, Shaanxi, and Shanxi. Tectonically, it forms part of the North China Craton and represents a typical foreland basin system. The well-preserved stratigraphic succession overlying the cratonic basement, combined with ample sediment supply and stable tectonic subsidence, has provided the basin with rich mineral resources [13–15]. Since the Paleozoic, the basin has evolved through five major developmental stages. During the Early Paleozoic (Middle Ordovician), the basin experienced marginal rifting and intracontinental subsidence, leading to the development of marine carbonate platforms. In the Late Paleozoic (Late Ordovician to Early Carboniferous), peripheral collisional orogeny caused basin-wide uplift and subsequent erosion. The subsequent Late Paleozoic (Late Carboniferous to Late Permian) was dominated by peripheral rifting under transitional marine-continental depositional systems. The Mesozoic stage was marked by intracontinental subsidence accompanied by marginal uplift and regional tilting, featuring fluvial, deltaic, and lacustrine sedimentation. The Cenozoic era was characterized by peri-basin faulted depression. The basin is subdivided into six first-order tectonic units: the Yimeng Uplift, Weibei Uplift, Tianhuan Depression, Yishan Slope, Jinxi Flexural Fold Belt, and Western Thrust Belt [16].

The western Sulige area is situated within the northern Tianhuan Depression, adjacent to the Western Thrust Belt (Figure 1). This region contains extensive Upper Paleozoic tight sandstone reservoirs exhibiting significant exploration potential. The primary gas-producing interval is the eighth member of the Lower Permian Shihezi Formation (He 8 Member). The Upper Paleozoic stratigraphic succession in the study area consists of, in ascending order: the Middle Carboniferous Benxi Formation, Upper Carboniferous Taiyuan Formation, Lower Permian Shanxi and Lower Shihezi Formations, and Upper Permian Upper Shihezi and Shiqianfeng Formations.

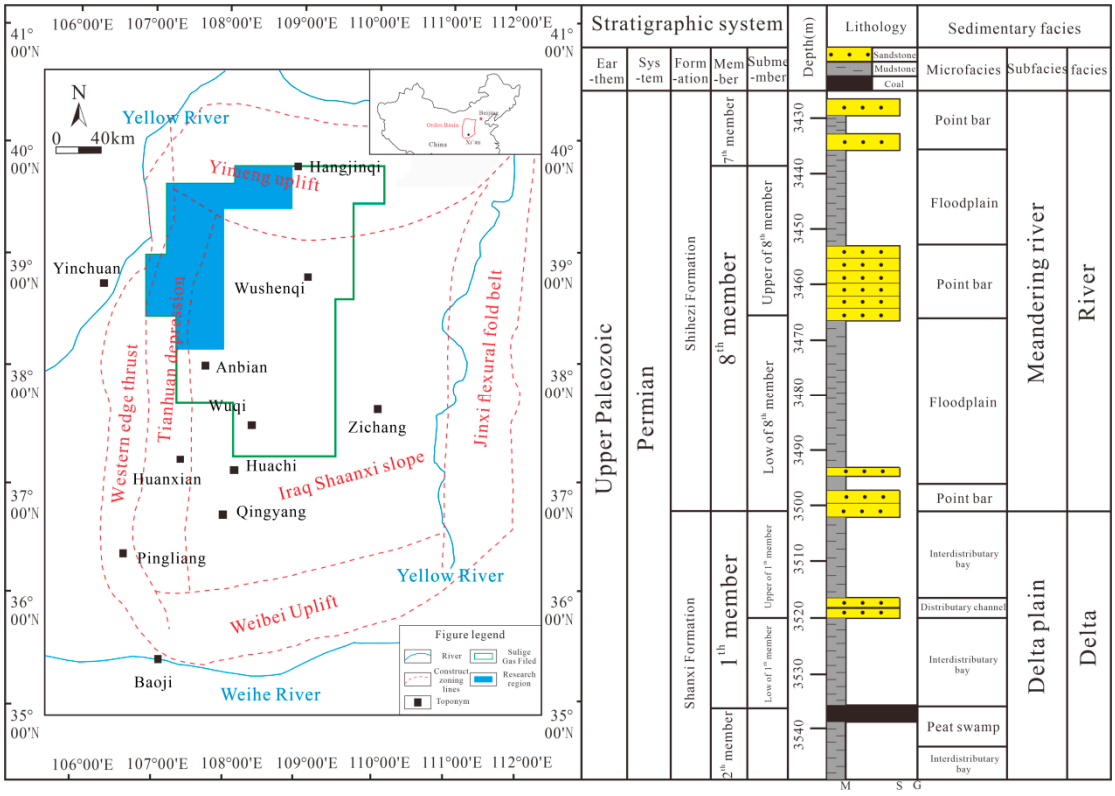


Figure 1. Structural location of the western Sulige area in the Ordos Basin and sedimentary characteristics of the Upper Paleozoic main gas-bearing intervals.

3. Materials and Methods

Based on a comprehensive review of previous literature, this study integrates drilling data, well logging, core observations, thin-section analysis, physical property measurements, and laboratory analyses. Techniques such as X-ray diffraction (XRD) and rock stress-sensitivity experiments were employed to investigate the He 8 Member of the Lower Shihezi Formation (Permian) in the western Sulige area of the Ordos Basin.

3.1. Sample Selection

The core samples used in this study were all collected from the He 8 Member in the western Sulige area of the Ordos Basin. Research on the reservoir characteristics in this region was supported by data from 486 wells within the study area.

3.2. Core Observation

Core observation and description constitute a meticulous geological foundation process essential for accurate lithological characterization. This process requires both comprehensive examination and focused attention on key characteristics. Analysis of core samples from the western Sulige area indicates that the He 8 Member is predominantly sandstone. The rocks are primarily light gray to grayish-white in color, with grain sizes ranging from fine to coarse (Figure 2). These sandstones display a hard texture, good sorting, and common argillaceous cementation, resulting in a densely consolidated structure. Based on systematic compilation and statistical analysis of core data, the sandstones were classified according to the four-component classification system.

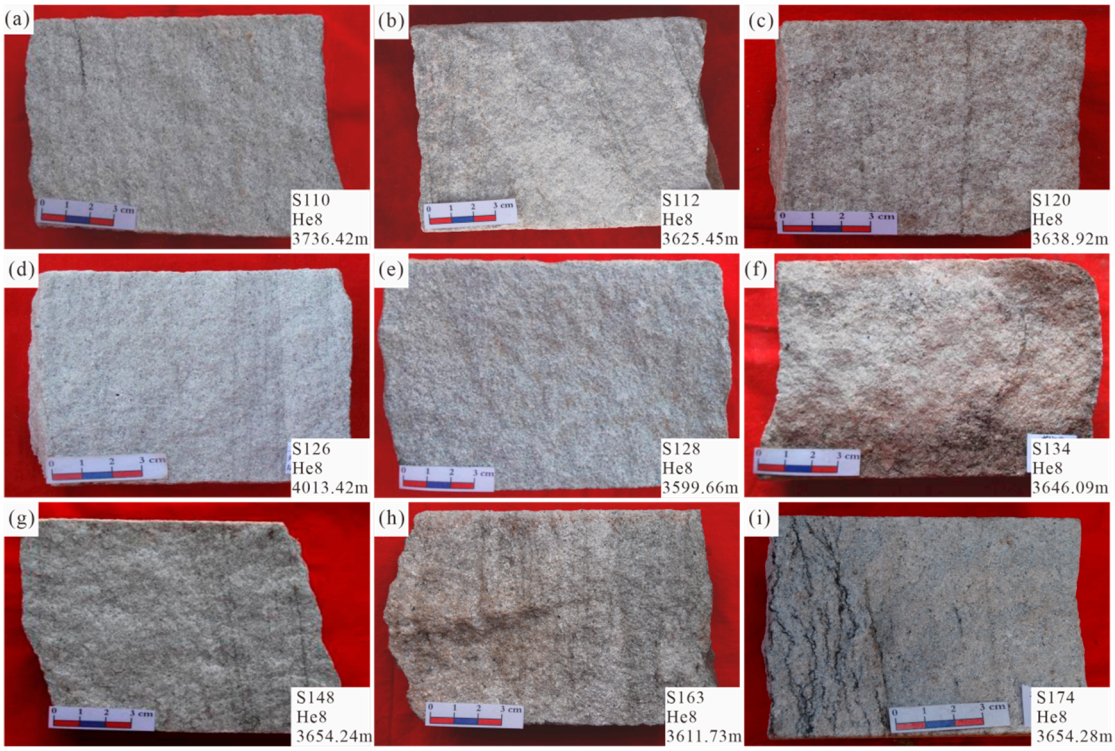


Figure 2. Core samples retrieved from the He 8 Member in the western Sulige gas field, Ordos Basin. (**a**) Grayish-white, medium-grained lithic quartz arenite, Well S110, 3736.42 m; (**b**) Gray, coarse-grained quartz arenite, Well S112, 3625.45 m; (**c**) Grayish-white, coarse-grained quartz arenite, Well S120, 3638.92 m; (**d**) Light grayish-white, fine-grained lithic quartz arenite, Well S126, 4013.42 m; (**e**) Light gray, medium-grained quartz arenite, Well S128, 3599.66 m; (**f**) Grayish-white, pebbly coarse-grained quartz arenite, Well S134, 3646.09 m; (**g**) Grayish-white, fine-grained quartz arenite, Well S148, 3654.24 m; (**h**) Grayish-white, medium-grained quartz arenite, Well S163, 3611.73 m; (**i**) Grayish-white, medium-grained quartz arenite, Well S174, 3654.28 m.

3.3. Microstructural Characterization

A total of 20 cast thin sections were prepared from the core samples. Following the Chinese industry standard SY/T 5368-2016 [17], all thin sections were examined and characterized using a DM4500P polarized light microscope (Leica Microsystems, Wetzlar, Germany) to investigate their mineral composition, pore structure, and reservoir morphology characteristics.

3.4. X-Ray Diffraction (XRD) Analysis

The X-ray diffraction experiment of whole rock and clay minerals was carried out according to the China Petroleum Industry Standard SY/T 5163-2010 [18]. The XRD equipment used was the German Bruker AXS D8-Focus X-ray diffractometer (Bruker, Karlsruhe, Germany). The sample state was solid powder, the environmental conditions were a temperature of 20 degrees Celsius and an air humidity of 32%, and the detection category was semi-quantitative analysis of the phase. The software used is XROCK XRD® (Ver 1.0). By identifying the characteristic peaks in the diffraction patterns, the author estimated the mineral content and clay mineral content in the samples.

3.5. Uniaxial and Triaxial Rock Stress Sensitivity Experiments

The stress sensitivity characteristics of reservoir rocks were evaluated using a triaxial rock mechanics testing system (Figure 3). This system was employed to simulate in

situ temperature and stress conditions, allowing for comprehensive measurements of mechanical properties, acoustic properties and compaction behavior.



Figure 3. Triaxial rock mechanics test system device.

I Liquid filling and emptying system; II HOEK Pressure Chamber; III Three-axis chamber pressure controller; IV Loading frame; V High-pressure injection pump; VI Servo hydraulic source; VII Com1&2.

Sample Preparation: Cylindrical specimens (diameter: 25.4 mm; length: 50.8 mm) were cut and polished to ensure end-face perpendicularity and parallelism within 0.02 mm. The samples were then encapsulated in heat-shrink sleeves and assembled into the triaxial pressure vessel for testing. Radial and vertical strains were measured using a cantilever-beam strain gauge (Beijing Sichuanger Building Testing Technology Development Co., Ltd., Beijing, China). Two types of experiments were conducted: uniaxial multi-cycle tests and triaxial multi-cycle tests.

Uniaxial Multi-Cycle Tests: For specimens with bedding planes oriented both parallel and perpendicular to the loading axis, axial load cycles (3–4 repetitions) were applied under negligible confining pressure (1 MPa holder pressure) until rock failure occurred. Strain parameters and fracture strength were recorded at each pressure increment.

Triaxial Multi-Cycle Tests: For a separate set of parallel- and perpendicular-bedding specimens, a confining pressure of 10 MPa was first applied, followed by 3–4 axial load-unload cycles until failure. Strain data and fracture strength were systematically documented.

The key technical parameters required for the experiment are shown in Table 1.

Table 1. Key technical parameters.

Parameter	Axial Stress Difference	Confining Pressure	Pore Pressure	Simulated Temperature
Unit	$\sigma d \leq 1470$ KN	$Pc \leq 140$ MPa	$Pp \leq 103$ MPa	$T \leq 200$ °C

4. Results

4.1. Lithological Characteristics of Reservoir Rocks

Core sample observations and statistical analyses (Figure 2) reveal that the Upper Paleozoic He 8 Member in the western Sulige area predominantly consists of sandstones with variable grain sizes, ranging from coarse to fine. A ternary diagram (Figure 4) was constructed using a four-component sandstone classification system to categorize the sandstone types [19] (Adapted and modified from Zhu., 2008). The results indicate that the target interval is primarily composed of quartz sandstones, followed by lithic quartz sandstones, with minor amounts of feldspathic quartz sandstones. Statistical analysis of sandstone types (Table 2) further demonstrates that: Quartz sandstones dominate, accounting for 78% of samples, Lithic quartz sandstones represent 27%, Feldspathic quartz sandstones comprise only 5%, Feldspathic lithic quartz sandstones are nearly absent.

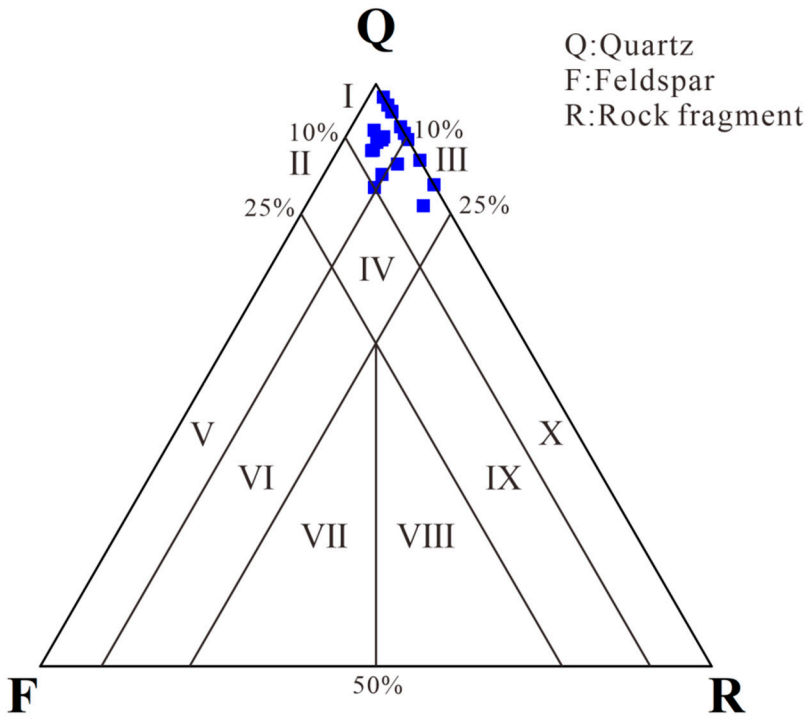


Figure 4. Classification of sandstone reservoirs in the He 8 Member, western Sulige area, Ordos Basin. I. Quartz Sandstone II. Feldspar Quartz Sandstone III. Lithic Quartz Sandstone IV. Feldspar Lithic Quartz Sandstone V. Feldspar Sandstone VI. Lithic Feldspar Sandstone VII. Rock Fragment Arkose VIII. Feldspar Lithic Sandstone IX. Feldspathic Lithic Sandstone X. Lithic Sandstone.

Table 2. Statistical distribution of sandstone types.

Sandstone Classification	Quartz Sandstone	Feldspar Quartz Sandstone	Lithic Quartz Sandstone	Feldspar Lithic Quartz Sandstone
Proportion	78%	27%	5%	<1%

4.2. Microstructural Characteristics of the Reservoir

The sandstone reservoir has experienced intense compaction and pressure dissolution, leading to tightly interlocked detrital grains and lithic fragments, along with varying degrees of quartz overgrowth. Primary intergranular porosity has been substantially reduced, with the pore system now dominated by diagenetically modified intragranular dissolution pores [20]. The development of secondary intergranular and intercrystalline micropores has further enhanced reservoir quality. In this study, thin sections of core

samples from the He 8 Member in the western Sulige area were examined using optical microscopy (Beijing Maite Micro Technology Co., Ltd., Beijing, China). The target interval exhibits well-developed secondary porosity, including dissolution pores, lithic dissolution pores, intergranular pores, and intercrystalline pores (Figure 5).

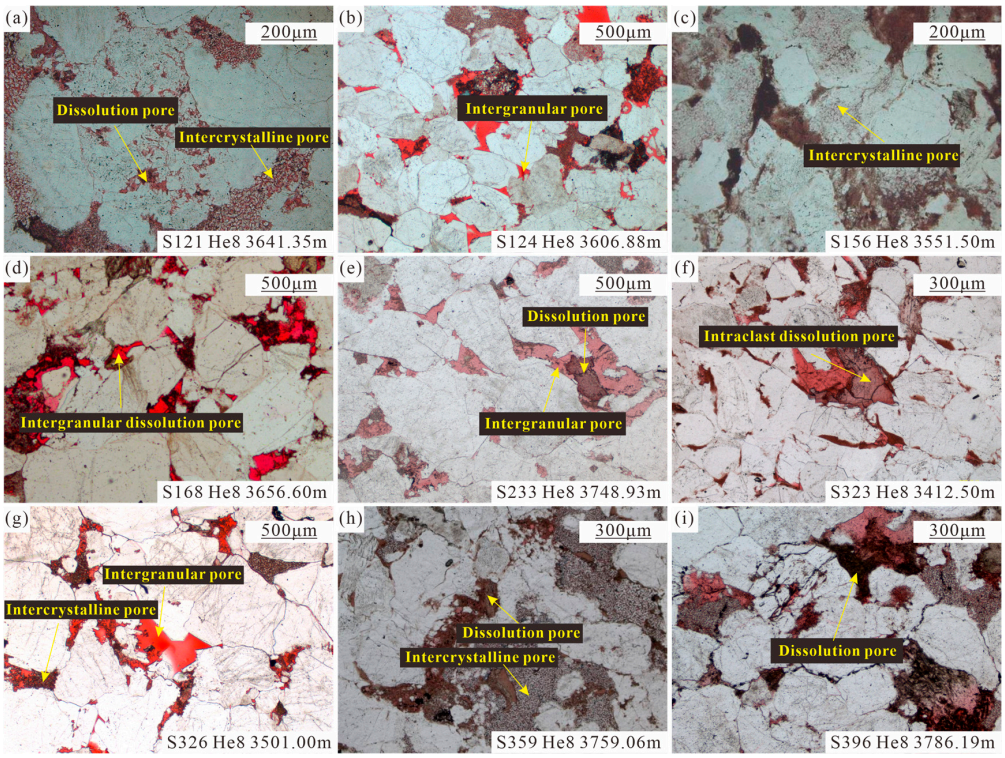


Figure 5. Photomicrographs showing microstructural characteristics of the He 8 Member sandstones, western Sulige area, Ordos Basin. (**a**) Intercrystalline and dissolution pores, Well S121, 3641.35 m; (**b**) Intergranular pores, Well S124, 3606.88 m; (**c**) Intercrystalline pores, Well S156, 3551.50 m; (**d**) Intergranular dissolution pores, Well S168, 3656.60 m; (**e**) Intergranular and dissolution pores, Well S233, 3748.93 m; (**f**) Lithic dissolution pores, Well S323, 3412.50 m; (**g**) Intergranular and intercrystalline pores, Well S326, 3501.00 m; (**h**) Dissolution and intercrystalline pores, Well S359, 3759.06 m; (**i**) Dissolution pores, Well S396, 3786.19 m.

The pore system is characterized by intergranular and dissolution pores ranging from 50 to 100 μm in diameter, which are commonly bitumen-filled. Pore preservation is controlled by the cementation degree, where residual intergranular pores persist in weakly cemented intervals. Acidic fluid activity has caused multistage dissolution of cement and matrix, generating secondary intergranular dissolution pores. Microscopic observations reveal complete cement dissolution and grain-edge dissolution features. Genetic analysis indicates this pore system represents a composite product of primary intergranular pores modified by diagenetic processes. Intercrystalline pores mainly occur in intensely recrystallized dolomites, displaying polyhedral morphologies with straight boundaries. Some have been modified by dissolution, forming intercrystalline dissolution pores. Microscopic analysis demonstrates that pore distribution is controlled by the original grain fabric rather than crystal alignment. Although recrystallization has redistributed the pores, it has not altered their fundamental intergranular characteristics. Notably, despite subsequent dissolution effects, the pore genetic mechanism remains predominantly controlled by sedimentary processes, while intragranular intercrystalline (dissolution) pores may be associated with burial-stage dissolution activities.

The rock interstitial materials consist primarily of matrix and cements. The matrix is composed of clay minerals and terrigenous clastic particles, while the cements are mainly

carbonate and silica-based. Thin section analysis reveals that clay minerals constitute the predominant interstitial component, accounting for over 30% of the total. Terrigenous clastics and carbonate cements show relatively lower proportions at approximately 20% each, with siliceous cements representing an intermediate proportion of 27%. X-ray diffraction analysis of the clay-sized fraction in the He 8 Member of the western Sulige area identifies four principal phyllosilicate minerals: kaolinite, illite, chlorite, and smectite (Figure 6). Among them, chlorite is the most abundant, reaching 40.77%, followed by kaolinite and illite at 20–30% each. The illite-smectite mixed-layer clay constitutes less than 10%, with an average proportion of only 8.14%. This particular clay mineral assemblage contributes positively to reservoir quality improvement.

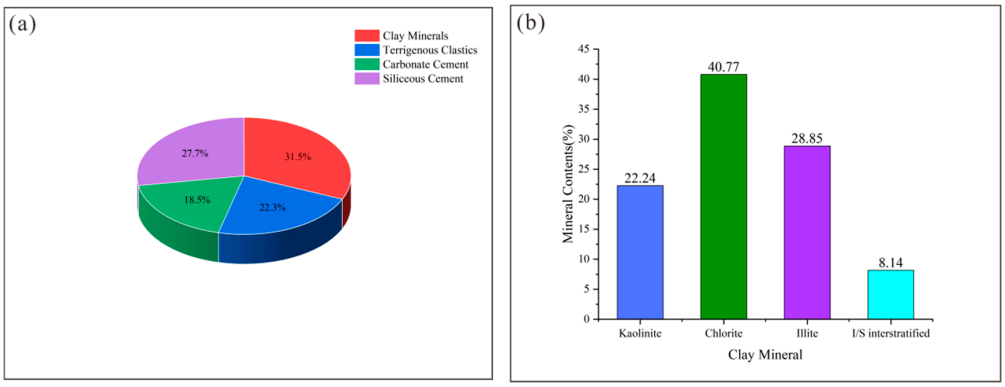


Figure 6. Microstructural characteristics of the Upper Paleozoic Ordovician-Permian Shihezi Formation reservoirs in the western Sulige area, Ordos Basin. (**a**)Types of interstitial materials; (**b**) Clay mineral composition.

4.3. Reservoir Physical Properties

The petrophysical analysis of the He 8 Member in the western Sulige area reveals a tight sandstone reservoir with generally low porosity and permeability characteristics. Porosity measurements range from 1.36% to 9.55%, with the majority of samples (85%) clustering between 2.0% and 8.0%, yielding an average porosity of 5.5% and median value of 5.6%. Permeability exhibits a wider variation from 0.004 to 1.3625 mD, though 95% of measurements fall within the 0.010–1.000 mD range, with mean and median values of 0.150 mD and 0.085 mD respectively (Figure 7). These parameters collectively characterize the reservoir as having low porosity and low-to-ultra-low permeability, with a compact structure and pronounced heterogeneity, typical of tight gas sandstone formations. A cross-plot of porosity versus permeability (Figure 8) demonstrates a strong positive correlation, further confirmed by linear regression analysis. This relationship suggests that porosity development is a key controlling factor for permeability in this tight sandstone reservoir.

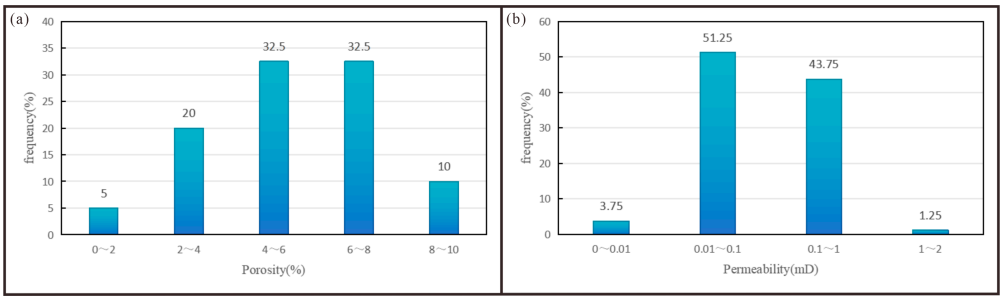


Figure 7. Frequency distributions of porosity and permeability in the He 8 Member, western Sulige area. (**a**)Porosity distribution; (**b**) Permeability distribution.

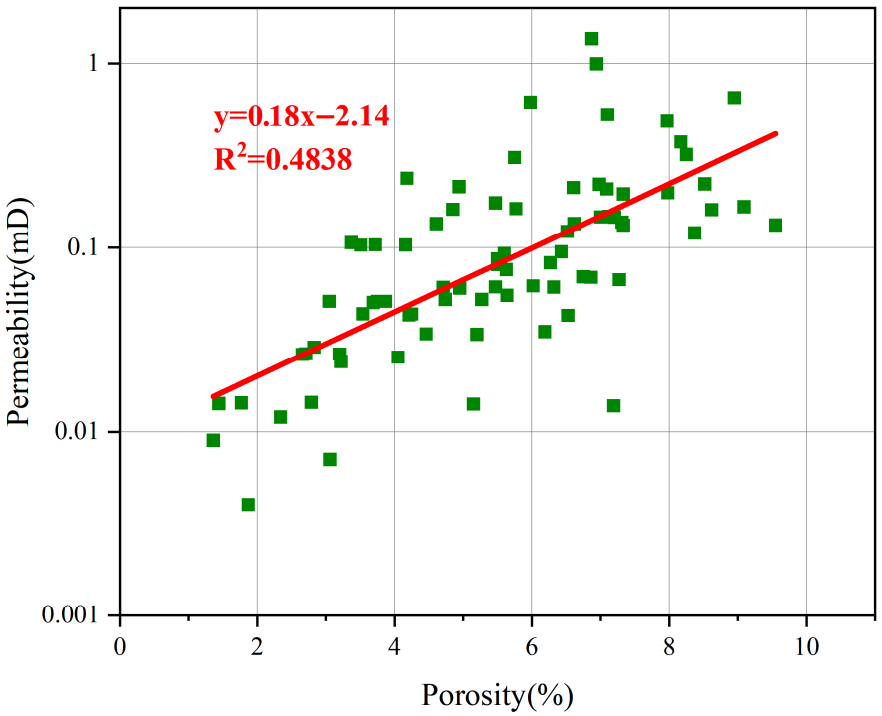


Figure 8. Porosity-permeability cross-plot of the He 8 Member sandstones, western Sulige area.

4.4. Rock Mechanical Characteristics

To systematically investigate the deformation, displacement, and fracture characteristics of the He 8 Member reservoir rocks, we conducted comprehensive mechanical tests on 16 core samples collected from 4 distinct depth intervals. The sample suite included both sandstone and mudstone specimens with different bedding orientations (parallel and perpendicular to bedding planes) (Table 3; Figures 9–12).

Table 3. Rock compression, rebound and fracture analysis data.

Well	Lithology	Depth (m)	Orientation (H-Parallel to Bedding Plane; V-Perpendicular to Bedding Plane)	Porosity (%)	Air Permeability (mD)
S117	Coarse-grained quartz arenite	3711.64	IH-1	13.4	1.33
			IV-1	13.2	1.65
			IH-2	14.9	1.61
			IV-2	14.4	1.92
S128	Medium-grained quartz arenite	3256.57	IIH-1	6.0	0.136
			IIV-1	10.1	0.183
			IIH-2	5.9	0.0755
			IIV-2	6.4	0.0825
S150	Mica-bearing fine sandstone	3469.15	IIIH-1	1.3	0.0486
			IIIV-1	1.3	0.0492
			IIIH-2	1.9	0.0391
			IIIV-2	2.4	0.0317
S164	Siltstone	3654.18	IVH-1	1.4	0.019
			IVV-1	0.7	0.022
			IVH-2	1.6	0.019
			IVV-2	0.8	0.016

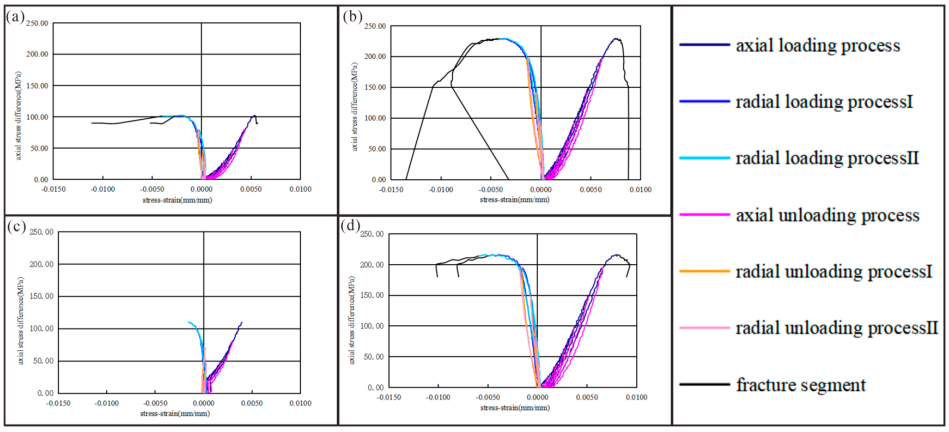


Figure 9. Stress–strain curves from compression, rebound, and fracture experiments on coarse sandstone samples. (**a**) H-1: Bedding-parallel, unconfined; (**b**) H-2: Bedding-parallel, high confining pressure; (**c**) V-1: Bedding-perpendicular, unconfined; (**d**) V-2: Bedding-perpendicular, high confining pressure.

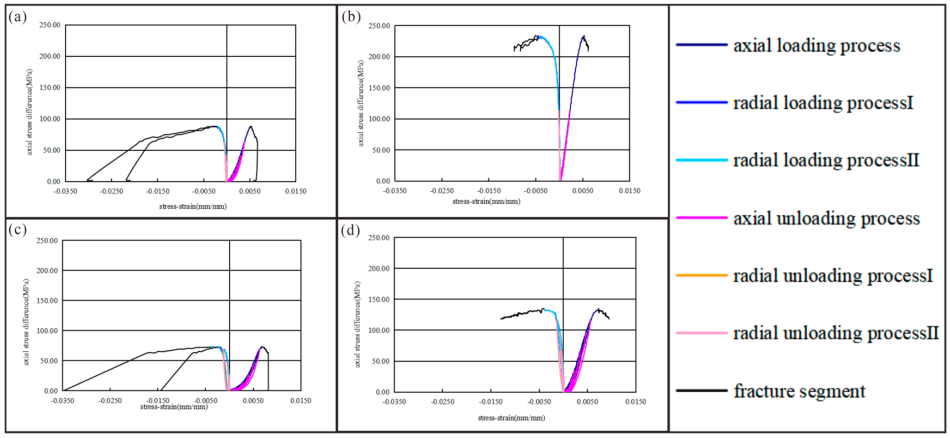


Figure 10. Stress–strain behavior of medium-grained sandstone during compression, rebound and fracturing experiments. (**a**) H-1: bedding-parallel orientation, unconfined condition; (**b**) H-2: bedding-parallel orientation, high confining pressure; (**c**) V-1: bedding-perpendicular orientation, unconfined condition; (**d**) V-2: bedding-perpendicular orientation, high confining pressure.

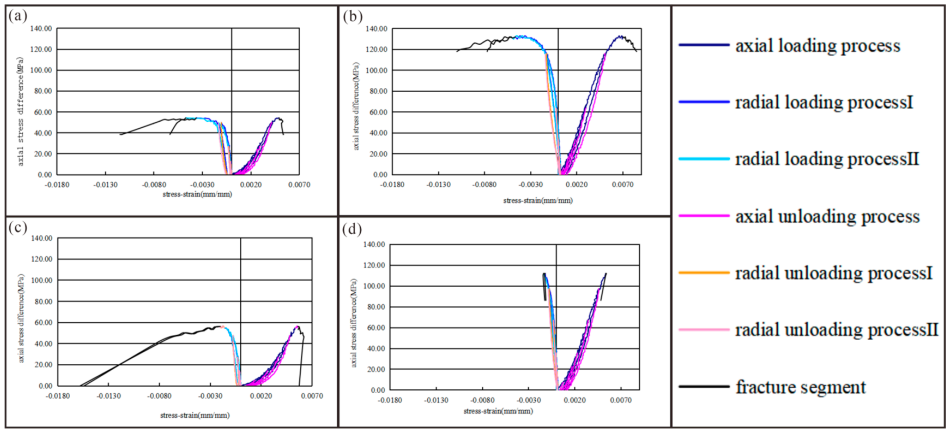


Figure 11. Stress–strain characteristics of fine-grained sandstone under compression, rebound and fracturing tests. (**a**) H-1: bedding-parallel, unconfined; (**b**) H-2: bedding-parallel, high confining pressure; (**c**) V-1: bedding-perpendicular, unconfined; (**d**) V-2: bedding-perpendicular, high confining pressure.

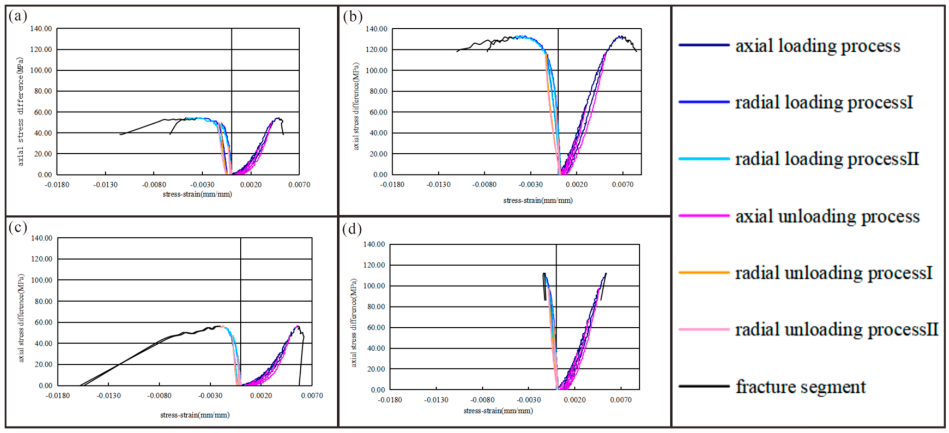


Figure 12. Stress–strain response of siltstone during compression, rebound and fracture experiments. (**a**) H-1: bedding-parallel orientation, unconfined condition; (**b**) H-2: bedding-parallel orientation, high confining pressure; (**c**) V-1: bedding-perpendicular orientation, unconfined condition; (**d**) V-2: bedding-perpendicular orientation, high confining pressure.

Under the same stress change conditions, the amount of compression and rebound in the parallel plane direction is less than that in the vertical plane direction. For example, for sample I, under 20 MPa pressure, the compressive strain value of H-1 (parallel layer, no confining pressure condition) is about 0.0024075 mm/mm, while the compressive strain value of V-1 (vertical layer, no confining pressure condition) is about 0.0035234 mm/mm. For the same type of rock samples, the confining pressure condition has an important influence on the compression and rebound of the rock. The general characteristic is that when the confining pressure increases, the axial strain value of the rock sample decreases and the fracture strength of the rock increases. For example, for sample I, when the compression strain is 0.002, the pressure of H-1 (parallel layer, no confining pressure condition) is about 15 MPa, while the pressure of H-2 (parallel layer, high confining pressure condition) reaches about 20 MPa.

The experimental results demonstrate distinct differences in fracture strength among rocks with varying structural characteristics (Table 4). Rocks exhibiting strong homogeneity perpendicular to bedding planes show higher fracture strength in the parallel-to-bedding direction compared to the perpendicular direction. Conversely, rocks displaying significant heterogeneity perpendicular to bedding demonstrate lower fracture strength in the parallel direction relative to the perpendicular orientation.

Table 4. Comparative analysis of compressive strength between bedding-parallel and bedding-perpendicular orientations.

Well	Lithology	Depth (m)	Rock Structural Characteristics (Vertical-to-Bedding)	Orientation H-Parallel to Bedding Plane; V-Perpendicular to Bedding Plane)	Unconfining Pressure Fracture Strength (MPa)	High Confining Pressure Fracture Strength (MPa)	Parallel-to-Bedding vs. Vertical-to-Bedding Strength Comparison	Porosity (%)	Permeability (mD)
S117	Coarse-grained quartz arenite	3711.64	Rocks with Strong Homogeneity	IH-1 IV-1 IH-2 IV-2	48.4 45.4	 119.1 116.3	H1 > V1 H2 > V2	13.4 13.2 14.9 14.4	1.33 1.65 1.61 1.92
S128	Medium-grained quartz arenite	3256.57	Rocks with Strong Homogeneity	IIH-1 IIV-1 IIH-2 IIV-2	72.7 54.5	 145.3 129.2	H1 > V1 H2 > V2	6.0 10.1 5.9 6.4	0.136 0.183 0.0755 0.0825
S150	Mica-bearing fine sandstone	3469.15	Rocks with Strong Heterogeneity	IIIH-1 IIIV-1 IIIH-2 IIIV-2	34.5 43.9	 94.4 120.5	H1 < V1 H2 < V2	1.3 1.3 1.9 2.4	0.0486 0.0492 0.0391 0.0317
S164	Siltstone	3654.18	Rocks with Strong Heterogeneity	IVH-1 IVV-1 IVH-2 IVV-2	43.6 63.2	 120.2 129.3	H1 < V1 H2 < V2	1.4 0.7 1.6 0.8	0.019 0.022 0.019 0.016

5. Discussion

5.1. Influence of Lithology on Reservoir Properties

The petrophysical characteristics of the He 8 Member tight gas reservoir are fundamentally controlled by its lithology and mineral composition. Dominated by quartz arenite with minimal development of unstable components such as lithic fragments and feldspars, the reservoir exhibits limited variability in physical properties.

X-ray diffraction analysis of detrital components reveals distinct relationships between mineral content and reservoir quality (Figure 13). While quartz content shows no significant correlation with porosity, reflecting the counteracting effects of silica cementation and pressure dissolution on pore space, feldspar content demonstrates a clear positive correlation. This relationship stems from feldspar dissolution creating intragranular pores that constitute a major component of the reservoir's porosity system. Consequently, higher feldspar abundance corresponds to a greater potential for dissolution and, thus, higher porosity. However, the overall scarcity of feldspar in the study area is a critical factor contributing to the tight nature of the reservoir.

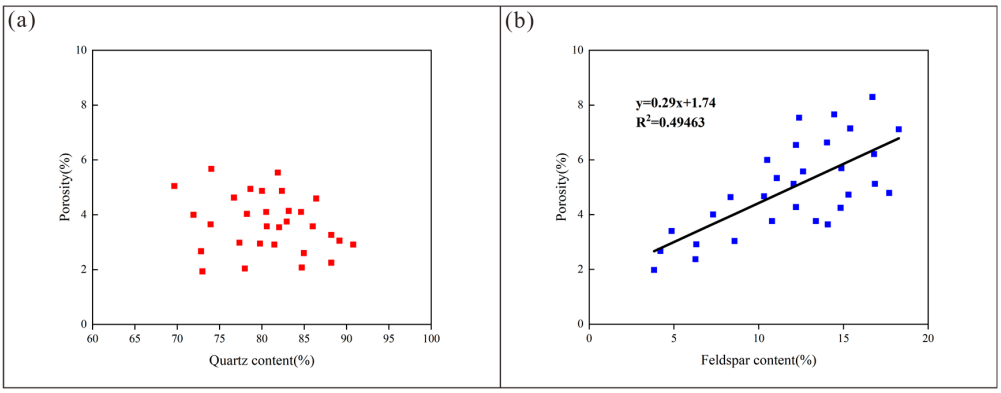


Figure 13. Correlation between detrital composition and porosity in the He 8 Member of the western Sulige area. (**a**) Relationship between quartz content and porosity; (**b**) Relationship between feldspar content and porosity.

The pore system in the study area, comprising dissolution pores, lithic dissolution pores, intergranular pores, and intercrystalline pores, likely results from the combined sedimentary input from multiple provenances in the northwestern, northern, and western margins of the basin. A marked contrast exists between the eastern and western sand belts in terms of their compositional and diagenetic characteristics.

The western sand belt exhibits quartz content exceeding 90%, with significant volcanic lithic fragments contributing to its distinctive dark gray coloration. This belt is characterized by kaolinite and illite as the predominant cements, yielding a pore network dominated by intergranular pores and intergranular dissolution pores. In contrast, the eastern sand belt, while similarly quartz-rich, contains higher proportions of metamorphic lithics and presents a light gray appearance due to widespread ferroan dolomite cementation, resulting in a pore system primarily composed of lithic dissolution pores and intercrystalline pores.

5.2. Sedimentary Facies Controls on Reservoir Development

The reservoir characteristics of the He 8 Member are fundamentally governed by sedimentary facies distribution, which was significantly influenced by the uplift of the northern Ordos Basin provenance area during the Lower Shihezi Formation deposition. This tectonic event provided substantial clastic sediments to the study area, forming three major sedimentary facies: alluvial plain, delta plain, and delta front (Figure 14).

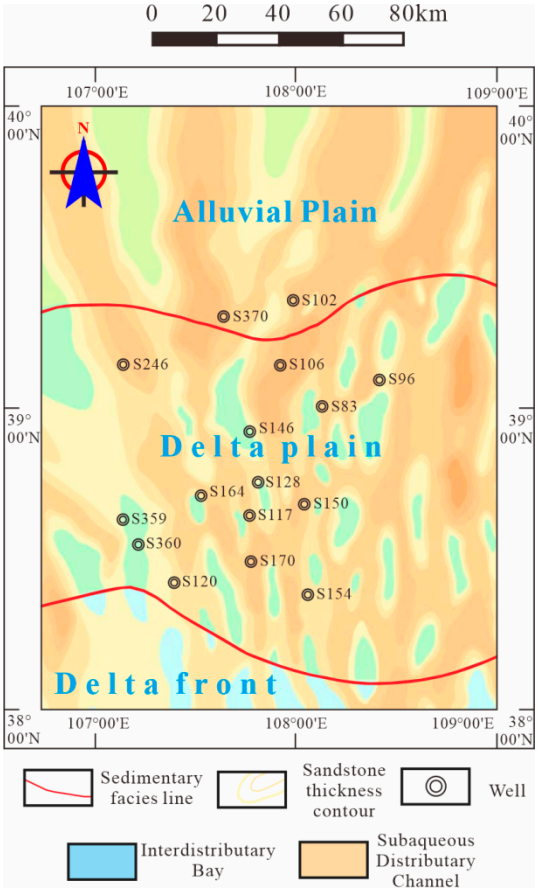


Figure 14. Sedimentary facies distribution of the He 8 Member in the western Sulige area.

A systematic analysis of sedimentary microfacies and petrophysical properties (Table 5) demonstrates clear facies-controlled reservoir quality variations in the western Sulige area. Subaqueous distributary channel deposits, representing the highest energy environment, develop the most favorable reservoir units with porosity generally exceeding 5.0%, though showing considerable permeability heterogeneity (0.01–1.0 mD). These channel sands form the primary exploration targets due to their well-developed pore systems. Moderate reservoir quality occurs in mouth bar deposits, characterized by more uniform porosity (3.5–4.5%) and permeability typically above 0.07 mD. In contrast, low-energy interdistributary bay and prodelta environments produce fine-grained sands and muddy siltstones with poor reservoir properties (porosity < 3.0%, permeability < 0.03 mD), representing non-prospective intervals.

Table 5. Relationship between sedimentary microfacies and reservoir properties in the He 8 Member of western Sulige.

Microfacies	Lithology	Sedimentary Structures	Porosity (%)	Permeability (mD)
Subaqueous Distributary Channel	Coarse Sandstone	Parallel Lamination	6.73	1.320
	Medium Sandstone	Massive Bedding	5.65	0.263
	Medium-Fine Sandstone	Massive Bedding	4.37	0.214
Mouth Bar	Medium-Fine Sandstone	Massive Bedding	4.26	0.148
	Fine Sandstone	Massive Bedding	3.82	0.073
Interdistributary Bay	Silty Sandstone	Horizontal Lamination	2.74	0.026
Delta Front	Siltstone, Mudstone	Horizontal Lamination	2.37	0.016

5.3. Effect of Diagenesis on Reservoir

In the process of burial depth, diagenesis has a great influence on the reservoir performance of sand bodies. The diagenesis in the western part of Sulige is complex, and the reservoir of the 8th member of Shihezi Formation has experienced a variety of diagenesis in the process of diagenesis. It mainly includes compaction, cementation, dissolution and fracture.

Compaction (Figure 5a–i) is the main reason for the reduction of primary pores in the study area. Evidence of compaction is present to varying extents in Figure 5a–i. In the sandstone of He 8 Member, the reservoir depth is large, the particle contact relationship is mainly linear contact and concave convex contact, and the particles are closely arranged. Especially in the middle sandstone, the content of plastic debris is high, and the plastic debris is compacted into a false matrix, which blocks the intergranular pores and significantly reduces the porosity of the reservoir. In addition, the silica dissolved in the particles can crystallize and precipitate to form quartz cements, which fill the pores in the form of quartz secondary enlargement or authigenic quartz crystals, further reducing the pore space and aggravating the densification of the reservoir.

The cementation (Figure 5b,d–g,i) of siliceous, kaolinite and ferrocalcite in the study area has played an important role in plugging reservoir pores. The multi-stage enlargement of quartz is obvious, and the uneven distribution of the enlarged edges around the particles can be seen. The strong quartz enlargement makes the particles in mosaic contact, which can cause the primary intergranular pores or secondary intergranular pores to be completely filled, resulting in the decrease or even disappearance of pores. Secondly, the authigenic kaolinite and ferrocalcite formed in the late stage filled some secondary intergranular pores, which destroyed the physical properties of the reservoir.

The dissolution (Figure 5b,d,g–i) can effectively increase the pore space of sandstone. The effective reservoir in the study area corresponds to the secondary pore development section, and the secondary dissolution pore is the main condition for the formation of effective reservoir. According to the observation of the cast thin sections, it is found that the dissolved components are mainly debris particles and some argillaceous interstitials, and the secondary pores are mainly particle dissolution pores formed by particle dissolution, which are more developed in coarse sandstone. The dissolution of matrix in He 8 Member is the most common and strong, and the dissolution strength is directly related to the content of matrix in interstitial materials.

Rupture (Figure 5d,f–i) is more developed in the 8th member of the study area, mainly caused by tectonic activity, forming structural fractures, with flat edges and zonal distribution. Rupture is usually manifested as micro-fractures passing through clastic particles. These micro-fractures will further develop into dissolution fractures in some sandstones, thus forming fracture-pore reservoirs. Fracture can form a fracture pore network in sandstone reservoirs, which can significantly improve the porosity and permeability of reservoirs. For sandstone reservoirs that are dense due to strong cementation and compaction, fracturing may be the only type of diagenesis that enhances pore space. In addition, the fracture action forms a rich fracture network, which can effectively communicate isolated pores, and can also be used as a migration channel of formation fluid, so that the acidic fluid can contact and react with the easily dissolved minerals, which significantly improves the physical properties of the reservoir.

5.4. Fracture Formation Characteristics of Tight Reservoir

The difference of compression ratio and fracture strength between parallel and vertical planes affects the formation of fractures in sandstone and mudstone.

Because under the same stress conditions, the compression and rebound, extension and shrinkage characteristics of different lithologies are different: the general order of compression strain and decompression rebound strain in parallel and vertical directions of coarse sandstone, medium sandstone, fine sandstone and argillaceous rock from high to low is: coarse sandstone > medium sandstone > fine sandstone > argillaceous rock. Therefore, in the combination of sand and mudstone, under the premise of certain burial conditions, the shrinkage rate of argillaceous rock parallel to the bedding plane is generally low, and cracks will be preferentially formed. At the same time, the sandstone is subjected to lateral shrinkage, which aggravates the densification of the sandstone. With the progress of horizontal shrinkage, the sandstone is broken accordingly. If the broken rock continues to squeeze and shrink, the rock will slide along the fracture surface to form a fracture with obvious slip marks (Figure 15).

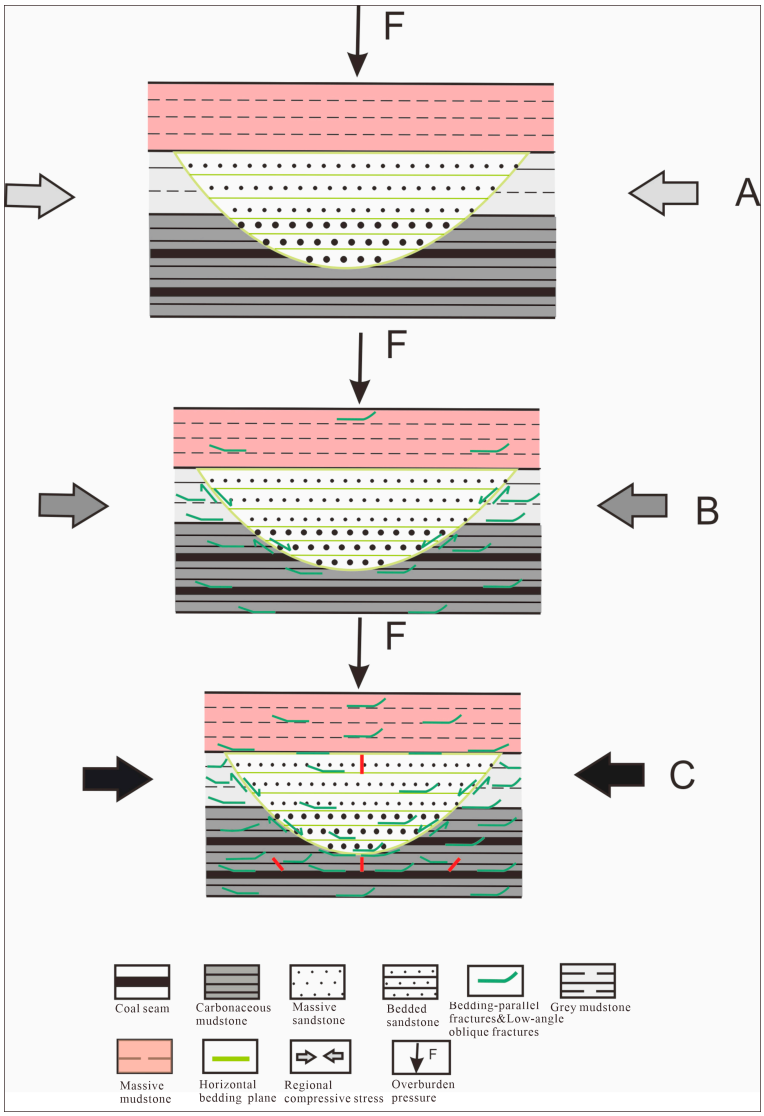


Figure 15. Conceptual model of fracture development during sandstone-mudstone compression.

6. Conclusions

The tight sandstone reservoirs of the He 8 Member in the western Sulige area exhibit characteristic low porosity and low permeability. The high quartz content limits the development of dissolution pores, leading to a pore system dominated by secondary pores and fractures.

Sedimentary microfacies are the key factors to control reservoir quality. Underwater distributary channel sand bodies have the best reservoir performance due to coarse-grained structure and high-energy sedimentary environment.

The reservoir has undergone complex diagenesis: early compaction and siliceous cementation lead to reservoir densification; the later dissolution and tectonic fracture effectively improved the reservoir physical properties.

Analysis of rock mechanical properties indicates that heterogeneous strata are more prone to fracturing under differential stress (σ_1–σ_3). These resultant fracture networks significantly enhance the seepage capacity of tight reservoirs.

Under the premise of certain burial conditions, the finer the grain size of the sandstone, the lower the shrinkage rate in the direction of the parallel plane, and the priority to form cracks. At the same time, the sandstone shrinks horizontally, which aggravates the densification of the sandstone reservoir.

This study addresses key scientific questions concerning the properties and fracture formation mechanisms of tight sandstone reservoirs in the He 8 Member (western Sulige area) through an integrated geological and rock mechanics approach. The findings can be directly applied to tight gas plays with analogous geological settings in the Ordos Basin, facilitating the prediction and assessment of favorable reservoirs. Areas where sedimentary microfacies (such as underwater distributary channels) overlap with fracture-developed zones should be prioritized as key targets for future oil and gas research. The relationships among "sedimentation diagenesis-mechanical response-fracture networks" revealed in this study provide critical theoretical support for enhancing the understanding of tight gas accumulation mechanisms and developing targeted technological solutions. Furthermore, this work offers a scientific basis for promoting the efficient and economical development of unconventional oil and gas resources.

Author Contributions: Conceptualization, J.Z. and Z.Z.; methodology, Z.Z.; validation, Z.C.; formal analysis, J.Z. and Z.Z.; investigation, W.W.; data curation, W.W.; writing—original draft preparation, Z.Z.; writing—review and editing, Z.Z.; visualization, Z.C.; supervision, J.Z. and Z.Z.; project administration, J.Z. All authors have read and agreed to the published version of the manuscript.

Funding: This research received no external funding.

Data Availability Statement: The data that support the findings of this study are available from the corresponding author, upon reasonable request.

Acknowledgments: This study was supported by technology and data provided by CNPC Changqing Exploration Institute.

Conflicts of Interest: The authors declare no conflicts of interest.

References

1. Ma, Y.; Cai, X.; Zhao, P. Theoretical understandings and practices of shale gas exploration and development in China. *Pet. Explor. Dev.* **2018**, *45*, 561–574. [CrossRef]
2. Zhao, J. Concepts, classification, and resource potential of unconventional oil and gas. *Nat. Gas Geosci.* **2012**, *23*, 393–406.
3. He, X.; Zhang, P.; Ren, J.; Wang, W.; Lu, B. Exploration and development practices of normal-pressure shale gas in the Dongsheng structural zone, Nanchuan area, southeastern Chongqing. *Pet. Geol. Exp.* **2023**, *45*, 1057–1066.
4. Jia, C.; Pang, X.; Song, Y. Mechanisms of unconventional hydrocarbon accumulation: Hydrocarbon self-sealing and intermolecular forces. *Pet. Explor. Dev.* **2021**, *48*, 437–452. [CrossRef]
5. Fu, J.; Dong, G.; Zhou, X.; Hui, X.; Dan, W.; Fan, L.; Wang, Y.; Zhang, H.; Gu, Y.; Zhou, G. Research progress of petroleum geology and exploration technology in Ordos Basin. *China Pet. Explor.* **2021**, *26*, 19.
6. Yang, H.; Fu, J.; Wei, X. Characteristics of natural gas accumulation in the Ordos Basin. *Nat. Gas Ind.* **2005**, *25*, 5–8.
7. Jin, X.; Mao, C.; Chen, Y.; Chen, Z. Analysis of reservoir characteristics and main controlling factors of He 8 member in Sudong area of The Sulige Gas Field. *Miner. Explor.* **2024**, *15*, 53–59.

8. Yang, T.; Zhang, G.; Liang, K.; Zheng, M.; Guo, B. Global progress in tight gas exploration and development and forecast of China's trends. *Strateg. Study CAE* **2012**, *14*, 64–68+76.
9. He, D.; Li, D.; Tong, X.; Wu, X. Theory of three-dimensional integrated hydrocarbon exploration in sedimentary basins of China. *Oil Gas Geol.* **2021**, *42*, 265–284.
10. Sun, L.; Zou, C.; Jia, A.; Wei, Y.; Zhu, R.; Wu, S.; Guo, Z. Development characteristics and orientation of tight oil and gas in China. *Pet. Explor. Dev.* **2019**, *46*, 1015–1026. [CrossRef]
11. Tian, B.; Yuan, Y.; Duan, Z.; Tang, J.; Qiu, S.; Zhang, J.; Guo, C. Sandy braided river tight sandstone reservoir characteristics and its main controlling factors-Taking the 8th member of Shihezi Formation in The Sulige Gas Field as an example. *Fault Block Oil Gas Field* **2024**, *31*, 387–394+402.
12. Sun, C.; Huang, W.; Liang, J.; Qian, L.; Zuo, Y.; Liu, F.; Liu, C. Tight sandstone reservoir characteristics and main controlling factors of He 8 member in Block 46 of The Sulige Gas Field. *Fault Block Oil Gas Field* **2024**, *31*, 97–206+215.
13. Yao, J.; Bao, H.; Ren, J.; Sun, L.; Ma, Z. Natural gas exploration under Ordovician salt beds in Ordos Basin. *China Pet. Explor.* **2015**, *20*, 1–12.
14. He, X.; Liu, C.; Wang, J.; Zhao, H.; Wang, F. Paleostructures of the Late Paleozoic in Ordos Basin. *J. Palaeogeogr.* **2011**, *13*, 677–686.
15. Zhao, Z.; Guo, Y.; Wang, Y.; Lin, D. Research progress on tectonic evolution and paleogeographic characteristics of Ordos Basin. *Spec. Oil Gas Reserv.* **2012**, *19*, 15–20+151.
16. Lu, S.; Yan, R.; Yuan, X. Reservoir characteristics and main controlling factors of He8 gas reservoir in southern The Sulige Gas Field. *Gas Explor. Dev.* **2012**, *35*, 1–4+81.
17. *SY/T 5368-2016*; Identification for Thin Section of Rocks. National Energy Administration: Beijing, China, 2016.
18. *SY/T 5163-2010*; Analysis Method for Clay Minerals and Ordinary Non-Clay Minerals in Sedimentary Rocks by the X-Ray Diffraction. Geology Exploration: Beijing, China, 2010.
19. Zhu, X. *Sedimentary Petrology*; Petroleum Industry Press: Beijing, China, 2008; pp. 109–114.
20. Liu, X.; Li, S.; Zhou, X.; Chen, X.; Liu, J.; Guo, Q.; Wei, J.; Liao, Y. New fields, new types and resource potential of oil exploration in Ordos Basin. *Pet. J.* **2023**, *44*, 2070–2090.

Disclaimer/Publisher's Note: The statements, opinions and data contained in all publications are solely those of the individual author(s) and contributor(s) and not of MDPI and/or the editor(s). MDPI and/or the editor(s) disclaim responsibility for any injury to people or property resulting from any ideas, methods, instructions or products referred to in the content.